Periodic solutions and chaos in the Barkley pipe model on a finite domain

K. Y. Short*
Center for Nonlinear Science, Georgia Institute of Technology, Atlanta, Georgia 30332, USA

(Received 10 May 2019; published 28 August 2019)

Barkley's bipartite pipe model is a continuous two-state reaction-diffusion system that models the transition to turbulence in pipes, and reproduces many qualitative features of puffs and slugs, localized turbulent structures seen during the transition. Extensions to the continuous model, including the incorporation of time delays and constraining the system to finite open domains—a trigger for convective instability—reveal additional solutions to the system, including periodic solutions and chaos unseen in the original $1+1$-dimensional system. It is found that the nature of solutions depends strongly on the size of the domain under study as well as choice of boundary conditions: on a finite domain for a particular window of parameter space, period doubling and chaos are observed.

DOI: 10.1103/PhysRevE.100.023116

I. INTRODUCTION

The subcritical transition to turbulence in canonical fluid flows sees two different behaviors at two different scales: fast turbulent (chaotic) fluctuations on a small spatial scale and long-lived alternating laminar-turbulent patches on a larger spatial scale (spatiotemporal intermittency). Recent results suggest that transitional turbulence is a chaotic transient with a superexponential distribution of lifetimes [1,2] consistent with the dynamical systems view of transient turbulence arising from a chaotic saddle in state space [2–6]. As the laminar solution for plane Couette flow is known to be linearly stable for all Reynolds numbers [7]—and numerical and experimental evidence suggests that this is likewise true for pipes [8–10]—the emergence of transient chaos (transient turbulence) must derive from a mechanism other than perturbation of the laminar flow [2]. For example, the following hypothesized chain of events can lead to the formation of a chaotic saddle that could sustain transient turbulence: Two steady states are created in a saddle node bifurcation. Linear stability analysis shows that the upper branch state is initially linearly stable. Next, a stable periodic orbit is created at a Hopf bifurcation. Eventually the orbit undergoes a period-doubling cascade and a chaotic attractor emerges. A boundary crisis destroys the attractor, after which it becomes a chaotic saddle that supports transient turbulence [3].

On a spatial scale much larger than that of chaotic fluctuations, the transition in pipes sees large-scale spatially intermittent *puffs* and *slugs*—localized turbulent structures—coexisting with quiescent background (laminar) flow [10]. Paradigmatic two-dimensional flows see localized structures analogous to those in pipes: regular spiral bands are observed in Taylor-Couette flows [11], and turbulent spot and stripe phases coexisting with a laminar background in plane Couette flow [12,13], forming Turing-like patterns evocative of those seen in Swift-Hohenberg systems and in several two-dimensional reaction-diffusion-advection systems. Manneville postulated that patterns observed in plane Couette flow, in particular, derive from a Turing instability, and remarks generally "[p]attern formation is indeed often an obliged stage in the transition to turbulence" [14].

Spatiotemporal patterns in fluid systems could result from Turing or Turing-Hopf instabilities. Barkley [15] proposed a minimal pipe model that reproduces many of the key features of puffs and slugs seen in numerical simulations and in experiments. Barkley's original model consists of two parts, each part addressing one of the two scales. First is a continuous reaction-diffusion model described by two coupled partial differential equations, whose dynamics we explore in this paper in hopes of identifying a telltale pattern-forming instability. The complement to the continuous system is a discrete model with a chaotic map that is invoked in the excited regime of parameter space to mimic the small-scale chaotic fluctuations seen in experiments and direction numerical simulations (DNS); a later version of the model replaces the discrete chaotic map with a continuous additive Gaussian noise [16]. Though Barkley's model is successful in predicting the transition to turbulence, it either invokes a discrete chaotic map to produce the requisite chaos [15] or introduces stochasticity to supply small-scale random fluctuations [16]. The success of the model, as well as its relative accessibility, compels further investigation.

In this paper, we show that chaos—including a route to chaos akin to that described in [3]—can be triggered in Barkley's continuous model with the inclusion of a small time delay and/or confining the dynamics to a finite open domain without need to resort to a complementary (chaotic) tent map. Additional new solutions emerge at a Hopf bifurcation to give rise to time-periodic states unseen in Barkley's original model. Further, it is argued that extending the model to two spatial dimensions (2D) (with zero flux boundary condition on the other dimension) should lead to stripes and spots, the hallmark Turing patterns seen in 2D systems.

*kyshort@gatech.edu

A. Models

Barkley's original continuous pipe model is

$$\frac{\partial q}{\partial t} + \overline{U}\frac{\partial q}{\partial z} = q[u + r - 1 - (r+\delta)(q-1)^2] + \frac{\partial^2 q}{\partial z^2} + \eta q\sigma,$$
$$\frac{\partial u}{\partial t} + \overline{U}\frac{\partial u}{\partial z} = \epsilon_1(1-u) - \epsilon_2 uq - \frac{\partial u}{\partial z},$$

where q is turbulence intensity and $u \in [0, 1]$ is the centerline velocity along the pipe axis $\hat{z}$ relative to the mean axial speed of the bulk $\overline{U}$. The η term is the adjunct Gaussian white noise introduced in [16] and σ the noise strength. The parameter r is analogous to the Reynolds number seen in the nondimensionalized Navier-Stokes equations.

In this paper, we follow Barkley's lead and transform to the $\overline{U} = 0$ frame that comoves with the steady bulk flow and replace the additive noise with fast dynamics h so that the system under study is

$$\frac{\partial q_{MF}}{dt} = f(q(t), q(t-\tau), u(t), u(t-\tau)) + \frac{\partial q(x,t)}{\partial z^2},$$
$$\frac{\partial u_{MF}}{dt} = g(q(t), q(t-\tau), u(t), u(t-\tau)) - \frac{\partial u(x,t)}{\partial z},$$
$$\frac{\partial h}{\partial t} = [\text{fast dynamics}]. \tag{1}$$

where

$$\begin{aligned} f &= f(q(t), q(t-\tau), u(t), u(t-\tau)) \\ &= q[u_\tau + r - 1 - (r+\delta)(q-1)^2] + \epsilon h \\ g &= g(q(t), q(t-\tau), u(t), u(t-\tau)) \\ &= \epsilon_1(1-u) - \epsilon_2 u q_\tau. \end{aligned} \tag{2}$$

Here q_{MF} and u_{MF} are regarded as time-averaged mean field variables operating on a slow timescale, h as small-scale deviations from the mean field whose dynamics occur on a faster timescale, and τ is the time delay—which may or may not be set to zero—so that $q_\tau = q(t-\tau)$ and $u_\tau = u(t-\tau)$. Focus is given to the large-scale behavior of q and u; consequently, we will set $h = 0$ and postpone fast timescale dynamics until the Discussion section.

The paper is organized as follows: numerical procedure; general results, including a discussion of the new periodic and chaotic solutions; a discussion of timescales in relation to percolation dynamics and the possibility of pattern-forming bifurcation in 2D.

B. Numerical procedure

For $z \in (0, N)$, the system under study is

$$\frac{dq}{dt} = f(q(t), q(t-\tau), u(t), u(t-\tau)) + \frac{\partial^2 q(x,t)}{\partial z^2},$$
$$\frac{du}{dt} = g(q(t), q(t-\tau), u(t), u(t-\tau)) - \frac{\partial u(x,t)}{\partial z},$$
$$\frac{\partial h}{\partial t} = 0 \tag{3}$$

initialized with

$$\left.\begin{aligned} q_o(\phi) &= \phi(\theta) \\ u_o(\psi) &= \psi(\theta) \end{aligned}\right\} \quad \text{for } \theta \in [-\tau, 0], \tag{4}$$

where $q_o(\phi), u_o(\psi) \in [0, 1]$ represent the initial turbulent and laminar intensities introduced into the inlet of the pipe. The dynamics are confined to a finite computational domain described by boundary conditions

$$\left.\begin{aligned} q(0,t) &= q(N,t) = 0 \\ u(0,t) &= u(N,t) + q(N,t) \end{aligned}\right\} \quad \text{for } t \in [0, T], \tag{5}$$

henceforth referred to as the smooth-inlet boundary conditions (SIBC).

The finite-difference method with $N \in (50, 1000)$ was used, where N is the number of spatial grid points in the domain, taken to be the length of the pipe under consideration, with spatial grid size $\Delta z = 0.2$. Time steps of $\Delta t = 0.05$ are default, but larger (e.g., $\Delta t = 0.1$) and smaller (e.g., $\Delta t = 0.025$) time steps were taken, too, as a check of the stability of the code. The linear portion of equations is solved implicitly to ensure numerical stability; the nonlinear portion is solved explicitly with Courant number $C < 1$. To accommodate a nonzero time delay $\tau \neq 0$, the system was solved at $t - \tau$ and the unphysical solutions found for $t < 0$ were discarded.

Stability of code was checked by (1) varying Δt and Δz and observing consistent behaviors with no amplification or waves; (2) comparing SIBC in a long pipe against periodic boundary conditions (PBC); it is observed that SIBC $\rightarrow$ PBC solutions for long enough domain; and (3) comparing solutions early in the time evolution before a boundary is encountered. As $N \rightarrow \infty$, periodic solutions destabilize and asymptotically approach the solutions seen in Barkley's original PDE model.

Smooth-inlet boundary conditions (SIBC) described in Eq. (5) were introduced as a proxy for constant mass flux boundary conditions in finite open pipe used in DNS and generated in laboratory settings: all flux leaving the domain, regardless of being in state q or u, is matched with an equal flux entering the domain as smooth flow u.

Parameter values $\epsilon_1 = 0.04$, $\epsilon_2 = 0.2$, and $\delta = 0.1$ are the same as those used by Barkley [15] and are fixed throughout. The parameter r is generally unrestricted, but focus is on the region of parameter space $0.7 \leqslant r \leqslant 1$.

II. RESULTS

The role of disturbances in the inlet of the simulated pipe was the motivation for the particular type of boundary condition used in this study. Smooth inlet boundary conditions (SIBC) were used here because it was felt they were truer to real pipes than periodic boundary conditions. Since intermittency depends on inlet conditions even in very long pipes [17], experimentalists aim for smooth flow in the entrance of the pipe so that the size of any perturbation can be known and controlled [1,10]. Further, real pipes are finite in length; fluid, be it turbulent or laminar, must advect out of the open end of a real pipe eventually. In a sense, the SIBC is a kind of model in and of itself, aiming to reflect pipe flows in real laboratory conditions.

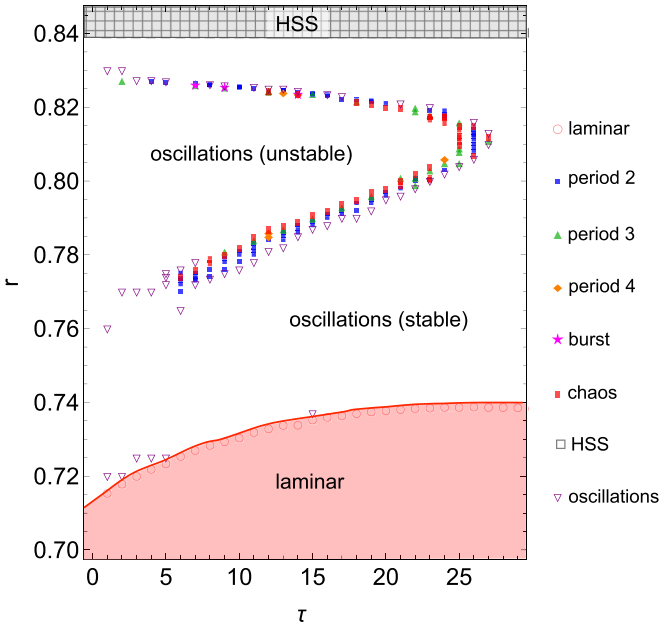

FIG. 1. Solution space at $N = 140$ as a function of time delay τ and r, where τ is number of time steps Δt. In this length of domain a variety of solutions is observed. A Hopf bifurcation first occurs in the undelayed system near $(\tau, r) = (0, 0.71)$; with increasing τ, the Hopf bifurcation occurs at increasing values of r, establishing a curve that defines the critical value τ_c above which periodic solutions are observed. Near $r = 0.839$, independently of τ, a final saddle-node bifurcation takes place whereby periodic solutions are destroyed and a homogeneous steady state (HSS) emerges (Fig. 2).

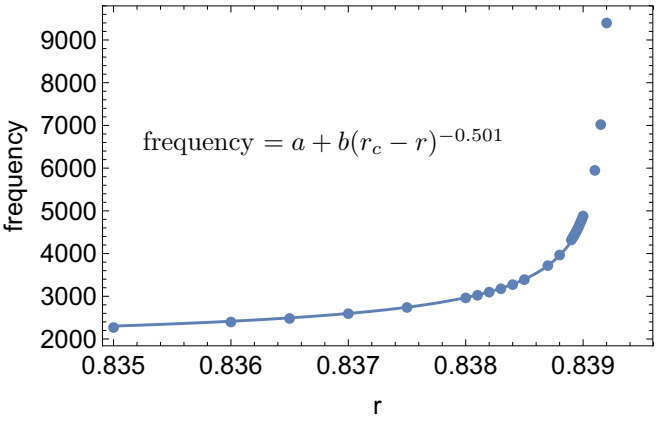

FIG. 2. Near the saddle-node bifurcation at $r_c \approx 0.839$, the frequencies of oscillation for q increase in accordance with the universal inverse square-root scaling law for saddle-node bifurcations. Shown is the best fit curve frequency $= a + b(r_c - r)^{-0.501}$, where $a = 1520$ and $b = 50.6$. This figure was drawn using data from $N = 500$.

While invoking SIBC, it is observed that solutions depend strongly on the length of the numerical domain N, in addition to the parameters r and τ. As the domain size N impacts the nature of the solutions, it may be treated as an implicit bifurcation parameter (see [18] for a treatment of domain length as an explicit bifurcation parameter). Thus the variable bifurcation parameters are $r(N)$ and $\tau(N)$. Houghton and Knobloch [19] discussed the role of boundary conditions in the Swift-Hohenberg equation subjected to finite domains: the system admits spatially periodic structures when subject to periodic boundary conditions (PBC), but sees large amplitude filling states when Neumann boundary conditions are imposed. The SIBC used here may be regarded as a hybrid of the two: absorbing for $q(z = N)$, periodic with an additional source for $u(z = 0)$.

With time delay and SIBC incorporated into Barkley's model, chaos is seen in a range of domain lengths at differing values of time delays—or, in the case of $N \approx 150$, at zero time delay—suggesting that the length of the domain plays a larger role in the observed solutions than does time delay. Figure 1 demonstrates the solutions that emerge at one set of parameters. For domains $N \approx 150$, a route to chaos follows a sequence of events remarkably similar to those thought to lead to transient turbulence in pipe [3]: Two coexisting steady states—a trivial "laminar" steady state with $q \to 0, u \to 1$, and a nontrivial excited steady state with $q \neq 0, u \neq 1$—are created at a saddle node bifurcation; the value of r for which this occurs depends on the amount of q introduced into the inlet of the system in analogy to a minimum perturbation amplitude required to transition from laminar flow [20]. Next, a Hopf bifurcation leads to sustained oscillations between the two coexisting steady states; no further perturbation or triggering beyond the initial condition is required to sustain the oscillations (Fig. 3). These periodic solutions are not observed in Barkley's original system. With increasing r and N, the amplitude of the stable limit cycles grows. Eventually, the periodic orbits undergo a period-doubling cascade (Figs. 4 and 5), followed by the emergence of a chaotic attractor (Fig. 6). With increasing r the chaotic structure disappears, and the stable periodic solutions give way to unstable periodic orbits that asymptotically decay to a nonlaminar steady state. As r is further increased for $N \sim 140$, chaos reemerges, this time accompanied by canard explosions ("bursts"): jumps from localized- to globally turbulent solutions that rapidly, but briefly, fill the whole domain; such solutions are unseen in the chaotic region at lower r. Beyond this, large amplitude oscillations are observed until the system undergoes another saddle-node bifurcation at $r \sim 0.839$ for all values of N studied, in agreement with Barkley's observation that the system undergoes a change somewhere between $r = 0.823$ and $r = 0.85$. Here, all periodic states are destroyed and only two homogeneous steady states—the trivial laminar and a large amplitude q steady state—remain. This regime is bistable and is identified with spreading puffs and global turbulence. The destruction of all stable periodic solutions occurs with the onset of the final saddle-node bifurcation. Beyond this point, the amplitude of q drops sharply before increasing again. Just before this final saddle-node bifurcation, the frequencies of the limit cycles approaches a "bottleneck," leading to increasing oscillation frequencies as the saddle-node bifurcation is approached [21]. We observe the universal inverse square root scaling law is obeyed, confirming the saddle-node bifurcation at $r = 0.839$ (Fig. 2).

All four behaviors—the two homogeneous steady states (HSS) and decaying and sustained oscillations—may be accompanied by initial transients. Long chaotic transients are most likely to be seen in the region between sustained oscillations and the slug HSS for $r \gtrsim 0.84$. These four

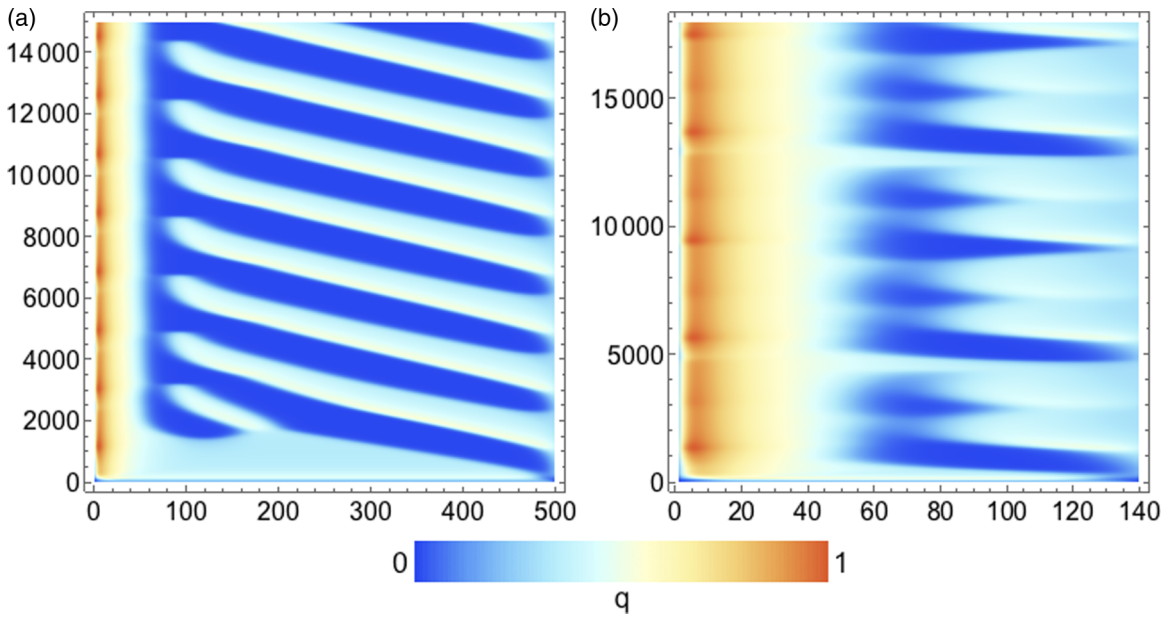

FIG. 3. Spacetime evolution of $q(z,t)$ in the $\overline{U}=0$ comoving frame with the spatial variable z on the horizontal axis and time t on the vertical. The inlet of the pipe ($z\sim 0$) can show relatively large initial turbulent transients. (a) Periodic solutions at $r=0.8274$, $N=500$, $\tau=0$. In a shorter domain, these same parameters result in canards (see Fig. 8). (b) A chaotic trajectory at $r=0.82$, $N=140$, $\tau=21$.

behaviors are seen elsewhere, for example, by Vanag and Epstein [22]. This is not too surprising given that Barkley's system, like Vanag and Epstein's, is a modified reaction-diffusion system. Further, as 2D reaction-diffusion systems often give rise to striping and other pattern formations, we suspect that Barkley's model can be extended to two spatial dimensions to model transitional stripelike structures seen in plane Couette and plane Poiseuille flows [23].

A. Periodic solutions

With SIBC, the modified Barkley model undergoes a Hopf bifurcation in every finite domain studied. Smaller domains (e.g., $N\sim 140$) see two sets of periodic solutions: a small-amplitude limit cycle at smaller r that eventually undergoes a period-doubling cascade and chaos, and a larger-amplitude limit cycle at larger r. Large domains (e.g., $N>300$) see large-amplitude limit cycles very soon after the initial saddle-node bifurcation, and only transient chaos. These "pulsating" [24] or "breathing" solutions are seen in domains with and without time delays, including $N=1000$, the largest domain studied here, and are reminiscent of breathing spots seen in 2D reaction-diffusion systems [25]. As $N\to\infty$, the periodic solutions grow unstable and we recover the asymptotic steady state solutions reported by Barkley [15].

The role of time delays in triggering Hopf bifurcations in $1+D$-dimensional systems and in Turing-Hopf transitions in 2D reaction-diffusion-advection systems has been studied previously. For example, Sen *et al.* [26] investigated the effect of small time delays in a pigmentation fish model and the chlorine dioxide-iodide-malonic acid (CDIMA) system, and Zhang and Zang [27] analyzed large delays in the extended Rosenzweig and MacArthur model with zero flux boundary conditions. Both groups observed a critical value of τ for the emergence of sustained Turing patterns. We make similar observations: there is a critical time delay τ_c above which instability sets in and below which the homogeneous steady states remain stable and no oscillations are observed. See Fig. 1.

B. Chaos

For finite domains subjected to SIBC, two sets of time-periodic solutions may be seen: a small-amplitude limit cycle (stable at lower r and N, unstable at larger r and N) and a large-amplitude limit cycle (unstable at small r and N). The former sees long-lived chaos, as well as chaotic transients, while the latter sees only chaotic transients, at least for the values of N and τ investigated in this paper. A period-doubling cascade and chaos is first encountered when a fixed-point solution collides with the small-amplitude periodic orbits, e.g., the onset of chaos near $r\approx 0.7873$, and $\tau=14$ for $N=140$. The crisis destabilizes the small-amplitude orbits, and the now-unstable periodic solutions decay asymptotically towards a nonlaminar steady state (however, at other values of N, chaos may still be observed at the same values of τ and r; see e.g., Fig. 7). As r increases further, another round of period doubling and chaos takes place. Interestingly, this time the chaotic solutions include canards and large-amplitude chaotic bursts: jumps from locally- to globally turbulent solutions that rapidly, but briefly, fill the whole spatial domain, perhaps analogous to random puff splitting events seen in pipes; such solutions are unseen in the earlier chaotic region at lower r. Other chaotic trajectories include visits to both coexisting orbits (see Fig. 8) and mixed-mode oscillations. Soon after, the small-amplitude limit cycles are destroyed, while the large-amplitude limit cycles stabilize. Consequently, the bifurcation diagram shows an abrupt jump to large-amplitude periodic orbits.

We note that the chaos described here is independent of any *ad hoc* chaotic tent maps; any fast timescale dynamics $h(t)$

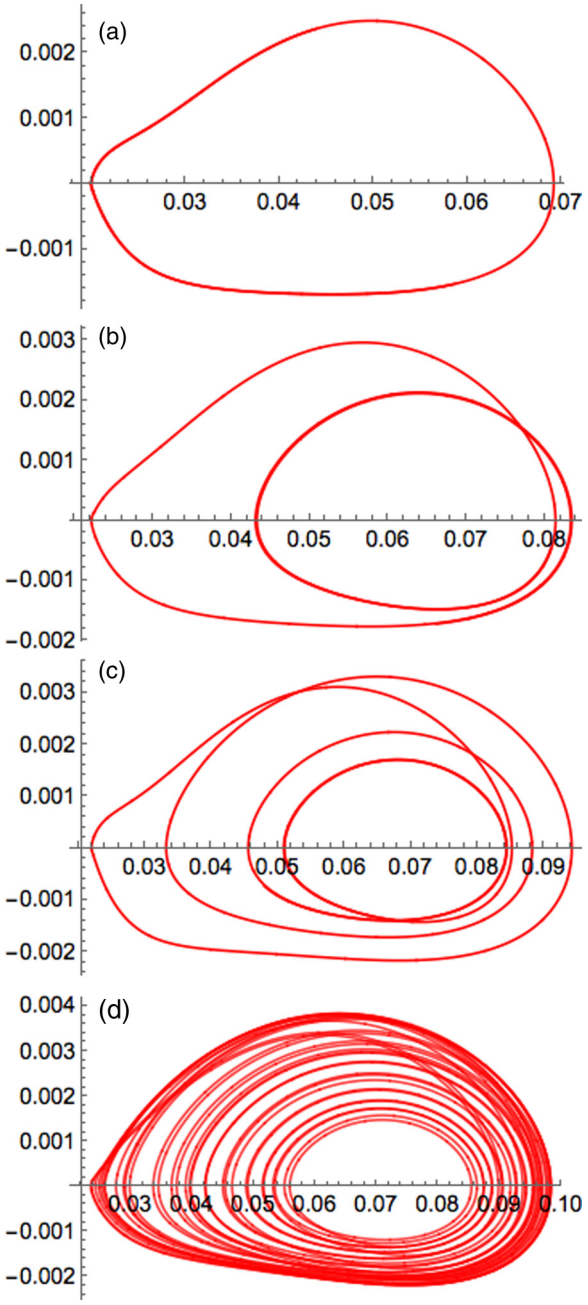

FIG. 4. Period-doubling route to chaos demonstrated in phase space, with q on the horizontal axis and $\dot{q}$ on the vertical. $N = 142$, $\tau = 7$, and (a) $r = 0.780$, (b) $r = 0.787$, (c) $r = 0.789$, and (d) $r = 0.79035$.

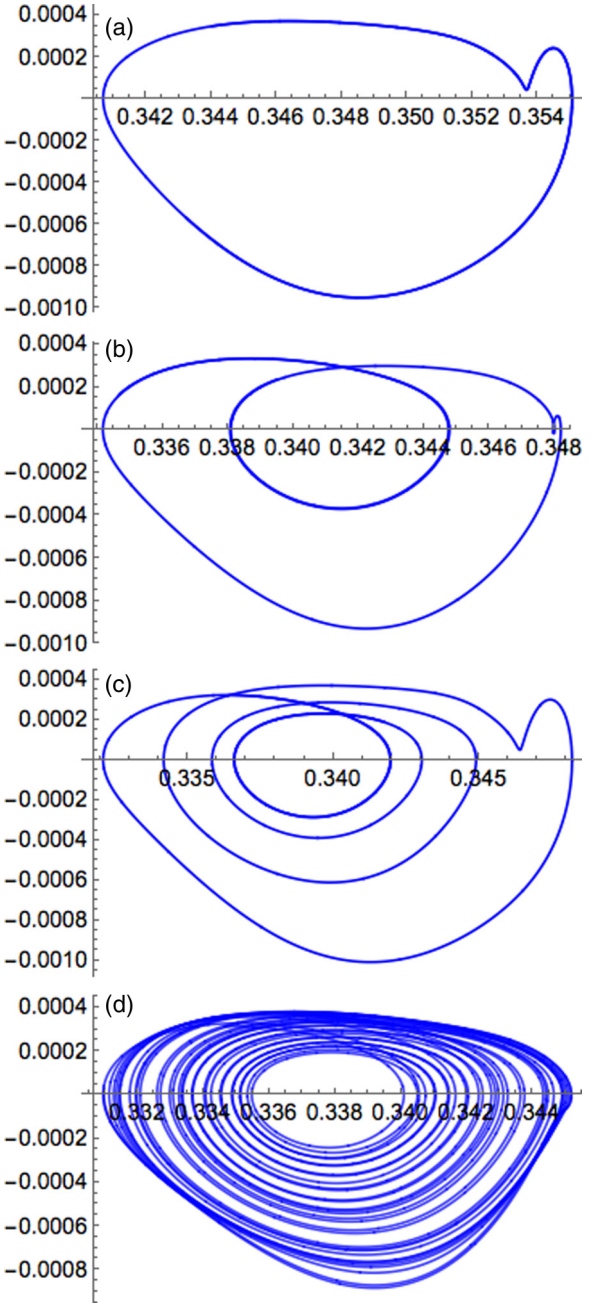

FIG. 5. Period-doubling route to chaos demonstrated in phase space with u on the horizontal axis and $\dot{u}$ on the vertical. $N = 142$, $\tau = 7$, and (a) $r = 0.780$, (b) $r = 0.787$, (c) $r = 0.789$, and (d) $r = 0.79035$.

superimposed or added to the system, including small-scale deviations from the mean-field values of q and u, will fluctuate chaotically due to the the chaos of the underlying slow system regardless of whether or not the fast dynamics described by $h(t)$ are chaotic.

III. DISCUSSION

The initial focus of this investigation was to understand the circumstances under which a pattern-forming instability and/or chaos could appear in Barkley's model, including the roles of boundary conditions and time delays known to affect pattern formation in other reaction-diffusion systems.

Pipe flow, like the Barkley model subject to the boundary conditions discussed in this paper, is an open system, and issues related to convective instability must be raised, including the possible presence of noise-sustained structures and concomitant spatiotemporal intermittency. For example, the transition from convective instability to absolute instability with increasing Reynolds number describes a mechanism by which a localized puff can become a spreading slug. As Deissler notes, any open system with nonzero group velocity

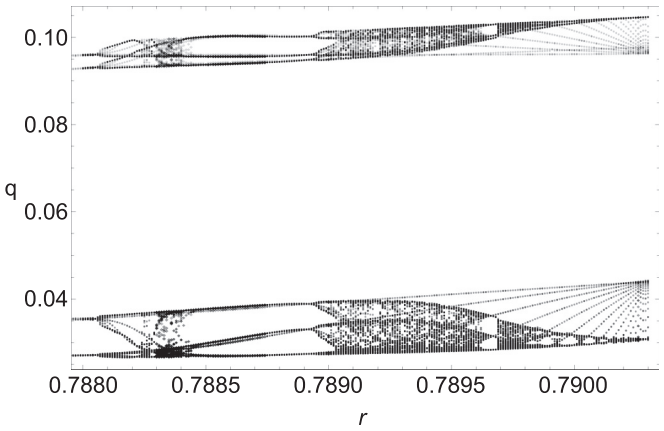

FIG. 6. Bifurcation diagram for the strongly chaotic region at $N = 140$; initial conditions are $q(t = 0) = 0.70$.

will be convectively unstable for some range of parameters [28]. Above the onset of an instability, the upstream and downstream front speeds of the localized perturbation will have the same sign as the group velocity, and a turbulent patch ("puff") will advect down the pipe, growing in the comoving frame of reference $\overline{U} = 0$.

Further, the open system can grow convectively chaotic, leading to the spreading of the turbulent structure ("slug"). For example, in the Ginzburg-Landau equation, when the amplitude of a perturbation near the fronts grows sufficiently large ("pops" into the chaotic basin of attraction), the slug will spread randomly in time. As the convectively chaotic fluctuations are effectively random, the information describing spreading slugs must be considered in the aggregate. Barkley *et al.* make an accordant observation of their data that the "bifurcation scenario predicted by the model is only recovered in

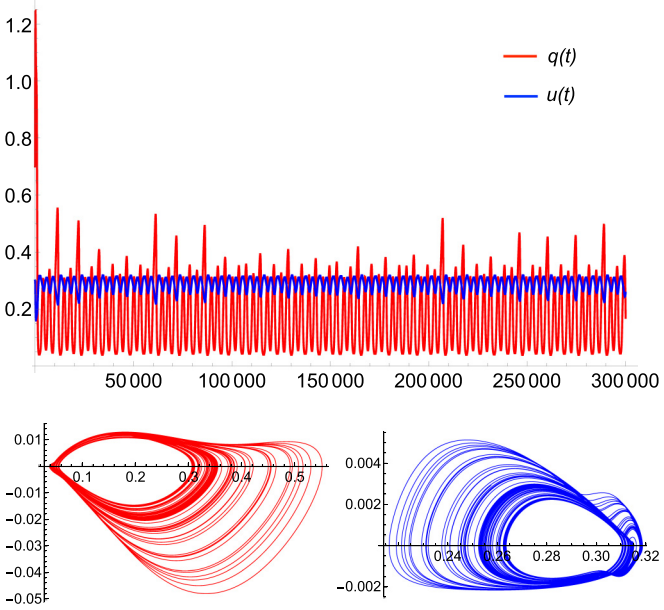

FIG. 7. Top: A chaotic time series at $r = 0.8176$ and $\tau = 22$ for $N = 140$. Bottom: The corresponding phase portraits: $(q, \dot{q})$ (red, bottom left) and $(u, \dot{u})$ (blue, bottom right).

average quantities" [29]. Barkley *et al.* acknowledge that the models—both the original form here as well as the amended form—fail to capture the stochastic fluctuations in the downstream front as well as the spatiotemporal intermittency in the whole of the domain ("intermittent laminar pockets"). Intermittency, too, can be ascribed to noisy fluctuations in convectively unstable systems, as noted by Deissler in an earlier paper [30].

Convectively unstable systems are especially sensitive to noise, and even small fluctuations can trigger large amplitude spatiotemporally varying structures and pattern formation in the whole domain [28]. Stochasticity—the random small scale variations that fluctuate the puffs, slugs, and their laminar-turbulent fronts—must be inserted into Barkley's model as an additional component operating at a faster timescale than q and u, but it is precisely these faster, smaller amplitude fluctuations that a convectively unstable system is sensitive to. Mullin, citing Waleffe [31], notes in his review that pipe flow becomes more sensitive to background disturbances as Reynolds number increases. Specifically, for a finite perturbation of amplitude ϵ, the minimum amplitude required to trigger turbulence scales with Reynolds number according to

$$\epsilon = \mathcal{O}(\mathrm{Re}^{\gamma}) \tag{6}$$

as $\mathrm{Re} \to \infty$ and $\gamma < 0$; that is, turbulence can be triggered with smaller and smaller amplitude disturbances as Reynolds number increases [10].

One approach proposed to describing small scale fluctuations $h(z, t)$ treats a turbulent patch—a puff or slug—as a directed percolation field. Experimental studies of the transition to sustained turbulence in Couette flow and in Waleffe flow was found to be consistent with a directed percolation process [32], and it is speculated that pipe flow, too, would fall into the directed percolation universality class [33]. With the directed percolation rules shown in Fig. 9 the resulting mean field equation for the percolating cluster is

$$\frac{\partial q_{MF}}{\partial t} \sim [\lambda(\mathrm{Re}) - \gamma)q - (k + \lambda(\mathrm{Re})]q^2 + D_z \frac{\partial^2 q}{\partial z^2}, \tag{7}$$

where a generic mean-field expression for q may be written down by balancing diffusion (with streamwise-directed diffusion coefficient D_z), the turbulence coagulation rate k, the reproduction/branching rate λ, and the $q \to u$ turbulent decay rate γ. Small fluctuations about q_{MF} would map to the faster, small-scale dynamics $h(z, t)$ in Eq. (1).

The appearance of the diffusion term in the percolation process is notable. (Barkley's original model neglected diffusion, effectively leaving $D_z = 1$, but his amended model incorporates a nonunit diffusion coefficient, e.g., $D_z = 0.13$ [29].) In general, the diffusive term inhibits short-wavelength perturbations; however, expanding the system to additional spatial dimensions may introduce pattern-forming instabilities, including diffusion-driven instability (Turing instability). In two dimensions with the bulk of the flow moving in the streamwise direction z and no net flow in the spanwise direction x, the two diffusivities would vary, with the D_z showing a streamwise bias and D_x without, setting up a situation ideal for pattern formation in 2D.

Diffusion through a percolating cluster, e.g., puff, differs from diffusion in a homogeneous medium. For a fractal

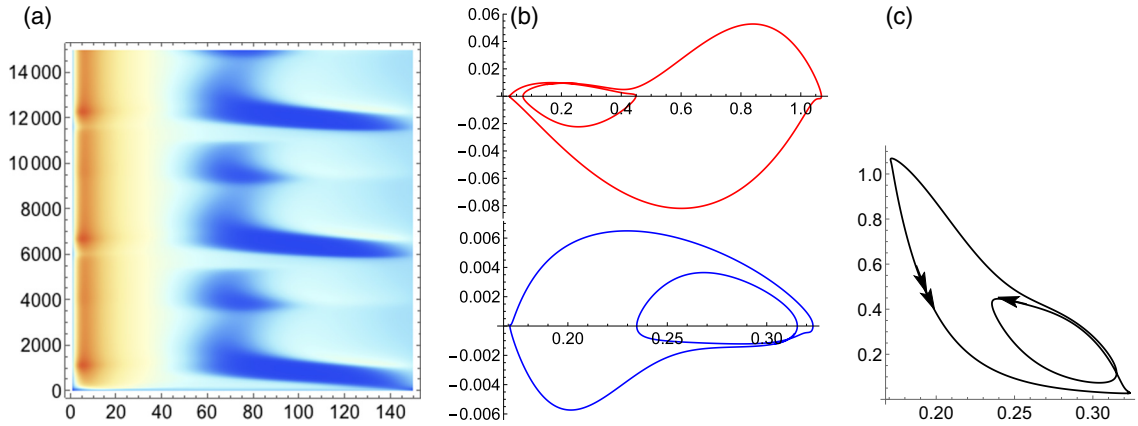

FIG. 8. Coexistence of small- and large-amplitude solutions at $r = 0.8274$, $N = 150$, $\tau = 0$. Canard behavior is observed when a trajectory, initially following the small-amplitude limit cycle, undergoes a fast excursion to the large-amplitude limit cycle before returning to the original orbit. (a) The spacetime evolution of $q(z, t)$; and the (b) phase space diagrams of $(q, \dot{q})$ (top) and $(u, \dot{u})$ (bottom) during the canard cycle. (c) A canard cycle in (u, q) space demonstrating orbits around the small-amplitude limit cycle with a quick excursion to a large-amplitude relaxation cycle. The small-amplitude limit cycle is destroyed at the saddle-node bifurcation at $r \approx 0.839$.

cluster or otherwise disordered medium, diffusivity depends on distance from percolation threshold p_c. Above the threshold ($p > p_c$) the cluster is effectively homogeneous and diffusion is regular, i.e., follows Fick's law $\langle R^2(t)\rangle \sim t^{2/d_w}$ with diffusion exponent $d_w = 2$. At criticality ($p = p_c$), however, the cluster is statistically self-similar at all length scales and the diffusion is anomalous with $d_w > 2$. Below criticality, $p < p_c$ the clusters are of finite size on the order of the correlation length $\xi(p)$ so that with $\langle R(t)\rangle^2 \sim \xi^2(p)$, where $\langle R(t)\rangle^2$ is the mean-squared displacement as $t \to \infty$ [34].

The percolation process here would be biased in the direction of the applied pressure gradient that is pushing the fluid through the pipe. There are two primary effects of this directional bias. First, the diffusion might show a nonzero drift velocity relative to the bulk velocity $\overline{U}$ [34]. Second, the pressure gradient may "trap" turbulent structures q at the boundaries of the cluster. To expand the turbulent cluster, the fluid particle must overcome the energetic barrier associated with the pressure gradient; that is to say, the particle must meet or exceed an energetic threshold in order for the turbulent structure to spread. Thus the spreading of puffs can be connected to Barkley's $u \to q$ transition rate so that $\epsilon_2(r)q_\tau$ must be analogous to a "threshold for excitation" and

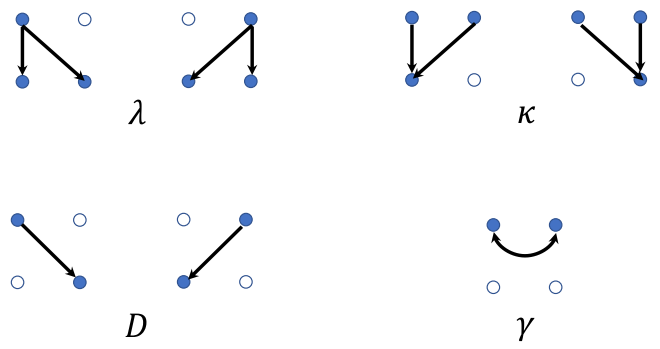

FIG. 9. Nearest-neighbor reaction-diffusion dynamics from time step t (top row) to $t + dt$ (bottom).

further connected to Goldenfeld's extremal fluctuations [35]. Since ϵ_2 is a function of r (or, in the directed percolation picture, the branching rate depends on Reynolds number) the fraction of the pipe filled with turbulence increases with Reynolds number. But percolation is not the only mechanism by which the turbulent structures can spread; convectively chaotic structures spread randomly, too.

SIBC were used here because it was felt they were truer to real pipes than periodic boundary conditions. Since intermittency depends on inlet conditions even in very long pipes [17], experimentalists aim for smooth flow in the entrance of the pipe so that the size of any perturbation can be known and controlled [1,10]. Further, real pipes are finite in length; fluid, be it turbulent or laminar, must advect out of the open end of a real pipe eventually. In a sense, the SIBC is a kind of model in and of itself, aiming to reflect pipe flows in real laboratory conditions.

While implementing boundary conditions, both smooth inlet boundary conditions (to model finite pipes) and periodic boundary conditions (to model an infinite pipe) were applied to see how solutions vary with finite domain size. When lengthening the domain while enforcing SIBC, we recover the solutions seen with periodic boundary conditions (PBC) and those found by Barkley. Consequently, one may view the new solutions—the time-periodic "pulsating" solutions and chaotic solutions, akin to those in [24]—to be additional sets of solutions seen in the limit of finite domains. That these time-periodic solutions grow unstable only at very large N suggests that SIBC induces a Hopf instability in the system, perhaps one that will interact with a Turing instability to bring about stripes in a two-dimensional extension of the model.

In addition, time-delayed coupling between u and q played less of a role in the set of observed solutions in this 1D model than did SIBC. However, the delay may play a bigger role in a two-dimensional extension of the model in accordance with literature on time-delay-induced Turing instabilities. One may anticipate that an extension of the model to 2D will generate spots and stripes like those seen in plane Couette flow, and similar to those described by Manneville [14].

IV. SUMMARY

We were able to find previously unknown periodic solutions and generate chaos in Barkley's pipe model with two physically motivated modifications: by admitting a time-delayed coupling between q and u, and by introducing SIBC.

ACKNOWLEDGMENTS

This material is based upon work supported by a National Science Foundation Graduate Research Fellowship under Grant No. DGE-0707424. The author thanks K. Wiesenfeld.

[1] B. Hof, A. de Lozar, D. J. Kuik, and J. Westerweel, Phys. Rev. Lett. **101**, 214501 (2008).
[2] B. Eckhardt, Procedia IUTAM **5**, 165 (2012).
[3] T. Kreilos, Ph.D. thesis, Philipps-Universität Marburg, 2014 (unpublished).
[4] Y. C. Lai and T. Tél, *Transient Chaos: Complex Dynamics on Finite Time Scales* (Springer, New York, 2011).
[5] H. Faisst and B. Eckhardt, J. Fluid Mech. **504**, 343 (2004).
[6] B. Hof, J. Westerweel, T. M. Schneider, and B. Eckhardt, Nature (London) **443**, 59 (2006).
[7] V. Romanov, Funct. Anal. Appl. **7**, 137 (1973).
[8] S. Grossmann, Rev. Mod. Phys. **72**, 603 (2000).
[9] A. Meseguer and L. N. Trefethen, J. Comput. Phys. **186**, 178 (2003).
[10] T. Mullin, Annu. Rev. Fluid Mech. **43**, 1 (2011).
[11] D. Coles, J. Fluid Mech. **21**, 385 (1965).
[12] A. Prigent, G. Grégoire, H. Chaté, O. Dauchot, and W. van Saarloos, Phys. Rev. Lett. **89**, 014501 (2002).
[13] D. Barkley and L. S. Tuckerman, Phys. Rev. Lett. **94**, 014502 (2005).
[14] P. Manneville, Europhys. Lett. **98**, 64001 (2012).
[15] D. Barkley, Phys. Rev. E **84**, 016309 (2011).
[16] D. Barkley, J. Phys.: Conf. Ser. **318**, 032001 (2011).
[17] V. Mukund and B. Hof, J. Fluid Mech. **839**, 76 (2018).
[18] V. Klika and E. A. Gaffney, Proc. R. Soc. A **473**, 20160744 (2017).
[19] S. M. Houghton and E. Knobloch, Phys. Rev. E **80**, 026210 (2009).
[20] B. Hof, A. Juel, and T. Mullin, Phys. Rev. Lett. **91**, 244502 (2003).
[21] S. H. Strogatz, *Nonlinear Dynamics and Chaos: With Applications to Physics, Biology, Chemistry, and Engineering* (Westview, Boulder, CO, 2014).
[22] V. K. Vanag and I. R. Epstein, Phys. Rev. E **71**, 066212 (2005).
[23] Y. Duguet, P. Schlatter, and D. S. Henningson, J. Fluid Mech. **650**, 119 (2010).
[24] V. Pimanov and N. Nikitin, paper presented at the Sixth International Symposium on Bifurcations and Instabilities in Fluid Dynamics, Paris, 2015 (unpublished).
[25] V. K. Vanag and I. R. Epstein, Chaos **17**, 037110 (2007).
[26] S. Sen, P. Ghosh, S. S. Riaz, and D. S. Ray, Phys. Rev. E **80**, 046212 (2009).
[27] T. Zhang and H. Zang, Phys. Rev. E **90**, 052908 (2014).
[28] R. J. Deissler, J. Stat. Phys. **54**, 1459 (1989).
[29] D. Barkley, B. Song, V. Mukund, G. Lemoult, M. Avila, and B. Hof, Nature (London) **526**, 550 (2015).
[30] R. J. Deissler, Phys. Lett. A **120**, 334 (1987).
[31] F. Waleffe, Phys. Fluids **9**, 883 (1997).
[32] M. Chantry, L. S. Tuckerman, and D. Barkley, J. Fluid Mech. **824**, R1 (2017).
[33] G. Lemoult, L. Shi, K. Avila, S. V. Jalikop, M. Avila, and B. Hof, Nat. Phys. **12**, 254 (2016).
[34] S. Havlin and D. Ben-Avraham, Adv. Phys. **36**, 695 (1987).
[35] N. Goldenfeld, N. Guttenberg, and G. Gioia, Phys. Rev. E **81**, 035304(R) (2010).